Optical Properties of Iron Pillared Clays as Catalysts for Heterogeneous Photo-Fenton Process

María A. De León,[†] Marta Sergio,[†] Juan Bussi,[†] Guadalupe Ortiz de la Plata,[‡] Alberto E. Cassano,[‡,§] and Orlando M. Alfano*[,‡]

[†]Laboratorio de Fisicoquímica de Superficies, DETEMA, Facultad de Química, Universidad de la República, Gral. Flores 2124, CC 1157, CP 11800, Montevideo, Uruguay

[‡]INTEC (Ingeniería de los Fotorreactores, Universidad Nacional del Litoral—CONICET), Colectora de Ruta Nacional N°168, Santa Fe, Argentina

ⓢ Supporting Information

ABSTRACT: Optical properties of iron pillared clays (Fe-PILCs) were determined by using spectrophotometer measurements coupled with the solution of the radiative transfer equation (RTE). The specific absorption and scattering coefficients, as well as the phase function for scattering, were obtained as a function of the wavelength in the range from 300 to 500 nm. Optical properties of the Fe-PILCs are greatly affected by their iron contents which are ascribed to changes in their textural properties and are significantly different from those of two other iron containing materials, goethite and zerovalent iron. To show an application of the optical properties, the quantum efficiency of the heterogeneous photo-Fenton process with a Fe-PILC was determined. The results indicate that Fe-PILCs could be used as catalysts in large-scale photoreactors whose dimensions could be adjusted in a wide range according to the catalyst load and iron content to be used.

1. INTRODUCTION

Advanced oxidation technologies (AOTs) have received wide interest as efficient techniques to treat waters containing highly toxic and recalcitrant pollutants. Pesticides, heavy metals, chlorinated hydrocarbons, dyes, disinfectants, and antibiotics can be easily transformed into inorganic compounds like water, carbon dioxide, and salts as final products. Reaction mechanisms involve the generation of $HO^{\bullet}$ radicals which are highly reactive and attack the organic matter in a nonselective form. Total mineralization usually appears to be unnecessary since intermediate compounds, e.g., carboxylic acids and aldehydes, are biodegradable and water treatment can be completed by conventional biological methods.[1−4]

Some of the most widely known AOTs are those named as Fenton and photo-Fenton techniques, in which the generation of $HO^{\bullet}$ radicals results from the reaction between H_2O_2 and Fe^{2+} in aqueous solution at temperature close to ambient conditions[5−7] according to

$$Fe^{2+} + H_2O_2 \rightarrow Fe^{3+} + OH^- + HO^{\bullet} \tag{1}$$

The irradiation of the solution with light of wavelengths up to 580 nm[8] also contributes to the generation of $HO^{\bullet}$ and the regeneration of Fe^{2+} by photolysis of the $Fe(OH)^{2+}$ complex:

$$Fe(OH)^{2+} + h\nu \rightarrow Fe^{2+} + HO^{\bullet} \tag{2}$$
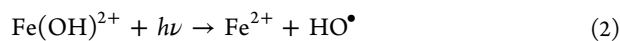
Because of the continuous regeneration of Fe^{2+} during the process, the iron salt plays the role of a catalyst added to the reactant system in nonstoichiometric and usually low amounts with respect to the other reactants.

In the past decade efforts have been made to develop solids displaying catalytic activity in photo-Fenton processes, thus allowing the simple recovery of the catalyst. Iron minerals or iron species supported on different solid materials (silica, alumina, zeolites, clays, activated carbon) have been tested as catalysts in photo-Fenton processes.[9−20] They have been tested with a wide variety of contaminants including dyes,[21] phenolic compounds,[22] pharmaceutical drugs,[9] agrochemicals,[23] and representatives of diverse industrial and municipal effluents.[24] Other materials based on manganese oxides[25,26] have been reported as effective heterogeneous catalysts in wet peroxide oxidation processes for contaminant degradation in aqueous solution.

As in homogeneous photo-Fenton reactions and other homogeneous photoactivated processes, the efficiency in the use of light is an important aspect to be evaluated in heterogeneous photo-Fenton systems, in which light scattering is an additional complexity factor. The efficiency of light utilization is formulated in terms of the quantum yield which relates the rate of the reaction and the rate of photon absorption as is common practice in homogeneous photo-chemistry. The calculation, as accurate as possible, of the local volumetric rate of photon absorption (LVRPA) is thus required, and this can be achieved by application of the radiative transport equation (RTE) for the proper determination of the radiation field inside the reactant system.

For rather dilute suspensions (pseudohomogeneous system) at ambient temperature (radiation emission is negligible) and for a single direction of propagation, the RTE can be expressed as[27,28]

$$\frac{dI_{\lambda,\Omega}(s,\,t)}{ds} + \kappa_\lambda(s,\,t)\,I_{\lambda,\Omega}(s,\,t) + \sigma_\lambda(s,\,t)\,I_{\lambda,\Omega}(s,\,t)$$

$$= \frac{\sigma_\lambda(s,\,t)}{4\pi} \int_{\Omega'=4\pi} p_\lambda(\Omega' \rightarrow \Omega)\,I_{\lambda,\Omega'}(s,\,t)\,d\Omega' \tag{3}$$

where $I_{\lambda,\Omega}(s,t)$ is the spectral specific radiation intensity along the directional coordinate s, with a wavelength λ and a direction of propagation $\underline{\Omega}$; κ_λ is the absorption linear volumetric coefficient, σ_λ is the scattering linear volumetric coefficient, and p is the phase function for spatial characteristics of the scattering phenomenon that acts as a source of photons coming from any direction $\underline{\Omega}'$ to the direction under consideration $\underline{\Omega}$. The parameters κ_λ, σ_λ, and p are optical properties which are characteristics of such solid materials.

With the knowledge of the optical properties (either from literature data or by experimental determination), the spectral and directional distribution of radiation intensities can be obtained by solving the RTE. Then the spectral incident radiation at a point located at the position $\underline{x}$ can be calculated by

$$G_\lambda(\underline{x},\,t) = \int_\Omega I_{\lambda,\Omega}(\underline{x},\,t)\,d\Omega \tag{4}$$

From eq 4, the local volumetric rate of photon absorption for polychromatic radiation is obtained by integration over the entire wavelength range of interest:

$$\text{LVRPA} = e^a(\underline{x},\,t) = \int_{\lambda_1}^{\lambda_2} \kappa_\lambda(\underline{x},\,t)\,G_\lambda(\underline{x},\,t)\,d\lambda \tag{5}$$

In the recent past, methodologies for the evaluation of optical properties has been applied to some solid materials used in photocatalytic and photo-Fenton processes (titanium dioxide, silica-supported TiO_2, goethite, and zerovalent iron nanoparticles).[17,29−32]

Pillared clays (PILCs) are solid materials which can incorporate iron, copper, and other transition metals and have shown catalytic activity for degradation of several pollutants in typical photo-Fenton conditions.[13] Iron pillared clays (Fe-PILCs) can be prepared by several techniques, and the resulting Fe species associated with the pillars have been reported as more effective and more resistant to leaching than other iron species. Recently a series of Fe-PILCs prepared by a simple technique with a montmorillonite without any other pretreatment than drying and sieving exhibited good catalytic properties in the degradation of dyes in typical photo-Fenton conditions.[33−35] Optical properties of Fe-PILCs have not been reported until now and their determination could help in better evaluation of their efficiency as catalysts in heterogeneous photo-Fenton processes.

In the present work the absorption and scattering coefficients and the phase function for aqueous suspensions of Fe-PILCs with different iron contents are evaluated. The determination of these optical properties implies (i) diffuse transmittance and reflectance spectrophotometric measurements of Fe-PILCs suspensions, (ii) evaluation of the radiation field in the spectrophotometer sample cell by resolution of the RTE for a one-dimensional system involving a single direction of light propagation, and (iii) application of a nonlinear multiparameter estimator coupled with an optimization program to adjust model predictions to experimental data. The results are compared with those obtained for goethite and zerovalent

iron nanoparticles, materials commonly studied as catalysts in heterogeneous photo-Fenton processes.

2. MATERIALS AND METHODS

2.1. Fe-PILCs Preparation. The starting raw material was a clay from Bañado de Medina, Uruguay. Over 80% of it is a calcium-rich montmorillonite with low sodium and potassium contents.[36] The cation-exchange capacity (CEC) determined by the ammonium acetate technique (1 M, pH 7) is 1.07 mequiv g^{-1} of dried clay. The clay was dried and ground, and the fraction of aggregate size less than 250 μm was selected by sieving and used for catalyst preparation.

The clay was exchanged with an aqueous solution of $[Fe_3(OCOCH_3)_7OH \cdot 2H_2O]NO_3$, prepared according to the method described by Yamanaka et al.[37] A solution of the iron complex was poured on an aqueous suspension (10% in weight) of the selected aggregate fraction of the clay until a final ratio of 0.5 mmol of complex g^{-1} of clay was attained. This procedure was repeated using 1.0 and 3.5 mmol of complex g^{-1} of clay. The exchanged clays were recovered by filtration, washed with deionized water, dried at 60 °C, and calcined at 400 °C in air atmosphere using a tubular furnace Carbolite CTF-12/65/550. The temperature was increased at 1 °C min^{-1} from room temperature up to 400 °C which was maintained for 2 h. The Fe-PILCs thus obtained were ground with a mortar and sieved. The particles that passed through a sieve of 200 mesh (nominal sieve opening 74 μm) were selected and denoted as C-0.5, C-1.0, and C-3.5 according to the complex/clay ratio used in the preparation.

2.2. Fe-PILCs Characterization. The iron content of the clay and of the catalysts was determined by energy dispersive X-ray fluorescence spectroscopy (EDXRF) in the "Laboratorio de Tecnogestión" of the Industry, Energy and Mining Ministry of Uruguay.

Nitrogen adsorption−desorption isotherms for the clay and the catalysts were determined at −196 °C in Micromeritics ASAP 2010 equipment. The specific surface area (S_{BET}) was determined from adsorption data using the BET model. The specific total pore volume (V_T) was determined from the adsorbed amount at a relative pressure of 0.95 transformed to volume of liquid, assuming a density of 0.808 g mL^{-1} for the adsorbed nitrogen. The specific micropore volume ($V_{\mu p}$) was determined using the Dubinin−Radushkevich model.

A Coulter LS230 was used for the laser diffraction particle size analysis. The instrument measures particle size in the range from 0.04 to 2000 μm. Analyses were done using water whose pH was adjusted at 3 as a dispersion medium, assuring the same conditions as used in optical properties determination, and with the Fraunhofer optical model as basis for the calculation.

2.3. Transmittance and Reflectance Measurements. Aqueous suspensions of the catalysts C-0.5, C-1.0, and C-3.5 were prepared employing different catalyst loads (C_{cat}) at pH 3: 0.2, 0.5, 1.0, 1.5, and 2.0 g L^{-1}. Measurements of collimated transmittance (T_λ), diffuse transmittance (DT$_\lambda$), and diffuse reflectance (DR$_\lambda$) of these suspensions were performed using an Optronic OL Series 750 spectrophotometer equipped with an OL 740-70 integrating sphere, measuring each 10 nm in the wavelength range from 300 to 500 nm. For each catalyst load and each wavelength, measurements were performed in triplicate. A flow cell with a pump that recirculates the catalyst suspension from a reservoir provided with a stirrer was used in order to avoid the sedimentation of the catalysts and keep a constant catalyst load in the measuring cell. The flow rate and

stirring were carefully adjusted to ensure the catalyst load value and the constancy of the particle concentration during the measurements.

2.4. Extinction Coefficient Determination. The extinction coefficient (β_λ) is a property of the solid suspension in water and is an extension of the absorbance property for homogeneous systems. For each catalyst load and each wavelength, β_λ was obtained from T_λ experimental measurements using the following equation:

$$\beta_\lambda = \frac{-\ln(T_\lambda)}{L} \tag{6}$$

where L is the cell path length.

The specific extinction coefficient as a function of wavelength (β_λ^*, β_λ per unit mass of catalyst load (C_{cat})) was obtained from the slope of a linear regression with forced intercept at the origin of the data β_λ versus catalyst load (C_{cat}) for each wavelength. The values obtained were used to compute the absorption coefficients as is explained in the following.

2.5. Methodology for Optical Properties Estimation. The optical properties were obtained adapting the corresponding method previously reported.[31] The RTE can be applied to a spectrophotometric cell under the following assumptions: (i) the cell is considered to be formed by two parallel plates separated by the cell thickness, (ii) the spectrophotometer receives an almost perfectly collimated beam of the incident radiation and the radiation field can be assumed to exhibit azimuthal symmetry, and (iii) the optical properties of the suspension are independent of time and position. With the above assumptions the simplified RTE becomes

$$\mu \frac{dI_\lambda(x, \mu)}{dx} + \beta_\lambda I_\lambda(x, \mu)$$
$$= \frac{\sigma_\lambda}{2} \int_{\mu'=-1}^{1} I_\lambda(x, \mu') \, p(\mu, \mu') \, d\mu' \tag{7}$$

Following the work of Satuf et al.[32] the Henyey and Greenstein (HG) phase function ($p_{HG,\lambda}$) was adopted for the radiation model in the spectrophotometer sample cell:

$$p_{HG,\lambda}(\mu_0) = \frac{1 - g_\lambda^2}{(1 + g_\lambda^2 - 2g_\lambda\mu_0)^{3/2}} \tag{8}$$

where g_λ is the dimensionless asymmetry factor defined as

$$g_\lambda = \frac{1}{2} \int_{-1}^{1} p_{HG,\lambda}(\mu_0)\mu_0 \, d\mu_0 \tag{9}$$

and μ_0 is the cosine of the angle between the incident and the scattered rays.

The effects of the reflecting walls of the spectrophotometer cell in the measurements were taken into account in the boundary conditions of eq 7:[31]

$$I_\lambda(0, \mu) = I_0\delta(\mu - \mu_0) + \Gamma I_\lambda(0, -\mu) \qquad (\mu > 0) \tag{10}$$

$$I_\lambda(L, -\mu) = \Gamma I_\lambda(L, \mu) \qquad (\mu < 0) \tag{11}$$

where Γ denotes the global wall reflection coefficient, δ is the Dirac delta function, and L is the spectrophotometric cell length.

The RTE (integro-differential equation) was solved numerically by the application of the discrete ordinate method (DOM).[38] This method was applied discretizing the wavelength λ, the spatial coordinate in the x dimension, and the

angle in the θ direction (represented by $\mu = \cos\theta$). Starting with plausible initializing values of κ_λ and g_λ to solve the equation, the theoretical results produced by the model for diffuse transmittance and diffuse reflectance are compared with the experimental values, using a nonlinear multiparameter estimator based on the algorithm of Levenberg–Marquardt. The procedure was repeated until the model was able to predict the experimental result, thus obtaining κ_λ and g_λ.

2.6. LVRPA Evaluation. The spatial distribution of the LVRPA as a function of the spatial coordinate x was evaluated for different catalyst loads of C-3.5 in a cylindrical perfectly stirred batch reactor with an inner diameter of 17 cm.[39] The bottom of the reactor was transparent (filter cutoff 300 nm) and illuminated with a tubular lamp (Philips TL'D 18W/08, emission range 340−410 nm) placed at the focal axis of a parabolic reflector. The net radiation flux at the reactor bottom experimentally measured by ferrioxalate actinometry was 5.65 × 10^{-9} einstein cm^{-2} s^{-1}.

3. RESULTS AND DISCUSSION

Iron content for the starting clay and the catalysts determined by EDXRF are shown in Table 1. The higher values for the

Table 1. Iron Content of the Clay and the Fe-PILCs

	Fe (% w/w)		
clay	C-0.5	C-1.0	C-3.5
1.1 ± 0.5	6.1 ± 0.5	13.4 ± 1.0	17.6 ± 2.5

catalysts with respect to that of the clay confirm that the iron complex was incorporated during the pillaring process. Moreover, the iron content for the catalysts increases with the complex/clay ratio used in the preparation.

Textural parameters for the clay and the Fe-PILCs are shown in Table 2. The specific surface area and the microporous

Table 2. Textural Parameters for the Clay and the Catalysts

solid	S_{BET} (m^2 g^{-1})	$V_{\mu p}$ (cm^3 g^{-1})	V_T (cm^3 g^{-1})
clay	31	0.013	0.049
C-0.5	56	0.023	0.057
C-1.0	111	0.046	0.069
C-3.5	130	0.051	0.099

volume (S_{BET}, $V_{\mu p}$) of the Fe-PILCs increased with increasing iron content, and for C-3.5 they become 4 times the values of the host clay.

These results depict the efficiency of the pillaring process here used to create a stable microporous structure in the clay by incorporation of iron species in the interlayer spaces of the clay. Changes in textural properties could affect the type and amount of active sites and thereby the rate of photon absorption and that of photochemical and chemical steps in the whole reaction mechanism.

The optical properties of the solids can depend on the particle size.[40] In order to evaluate such a possible correlation, results for particle size distribution based on volume for the three Fe-PILCs are presented in Figure 1. Table 3 includes the corresponding statistical information. As can be observed, the distribution covers a similar range with a scarce contribution of particles with size over 74 μm (sieve opening used for fraction selection). Only small differences in the particle size distribution for the catalysts are observed. Therefore, a marked
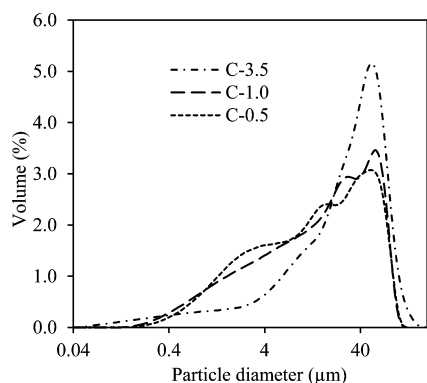
Figure 1. Particle size distribution for Fe-PILCs suspensions.

Table 3. Statistics of Particle Size Distribution for Fe-PILCs Suspensions

	catalyst		
statistical param	C-0.5	C-1.0	C-3.5
mean (μm)	24.60	25.95	36.95
median (μm)	15.64	17.96	32.97
mode (μm)	55.14	60.52	55.14
95% conf limit (μm)	0–72.24	0–74.04	0–92.49
SD (μm)	24.30	24.54	28.34

influence of this parameter in the optical properties of the Fe-PILCs is not expected. However, structural differences in Fe-PILCs with increasing iron content, as in this case, have been reported mainly related to changes in the long-range layer stacking; therefore, they could also affect both absorption and scattering properties.

For each wavelength, over the range of catalyst load studied (from 0.2 to 2.0 g L^{-1}), the plot of β_λ versus the catalyst load (C_{cat}) provided a good linear fitting through the origin for all the catalysts, as can be observed in Figure 2 for the case of 360 nm.

Figure 3 shows the values of β_λ* as a function of the wavelength obtained for C-0.5, C-1.0, and C-3.5. For all the catalysts, there are no significant variations of β_λ* in the wavelength range from 300 to 500 nm. The increase of iron
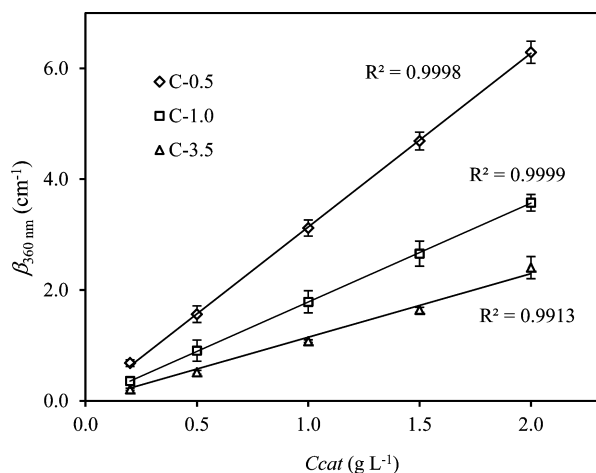

Figure 2. Linear regressions between the extinction coefficient and the catalyst load at 360 nm for the catalysts. Bars represent a 95% confidence interval.
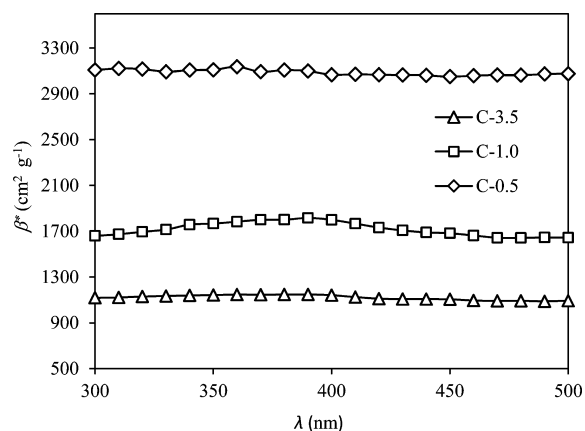

Figure 3. Specific extinction coefficient for the catalysts as a function of wavelength.

content in the catalyst leads to lower specific extinction coefficients for the whole range of wavelength studied, from 3066 to 3136 cm^2 g^{-1} for C-0.5 to 1088–1148 cm^2 g^{-1} for C-3.5. As reported in Table S1 in the Supporting Information, these results involving both absorption and scattering components of the radiation are intermediate between those of goethite (133–161 cm^2 g^{-1}) and zerovalent iron (ZVI) (22 496–24 216 cm^2 g^{-1}). These differences can be related to those of light–solid interactions by absorption and scattering phenomena. On one hand, light absorption should be related to energy transitions of the surface-exposed species. On the other hand, light scattering should be dependent mainly on morphological aspects of the solid including particle size and shape.

The comparisons between the predictions produced by the theoretical model and the experimental values of diffuse transmittance and diffuse reflectance measurements allowed the determination of κ_λ and g_λ values.

The specific absorption coefficient (κ_λ*) per unit catalyst load was obtained by applying a linear regression on the data κ_λ versus C_{cat}. Specific absorption coefficients (κ_λ*) of Fe-PILCs are shown in Figure 4 (see Table S2 in the Supporting Information). Light absorption is observed for the three catalysts over the entire wavelength range, although significant differences are observed between them when comparing κ_λ*
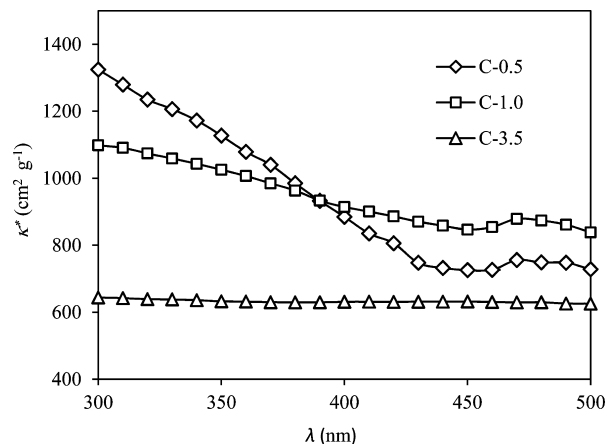

Figure 4. Specific absorption coefficient for the catalysts as a function of wavelength.

dependence on λ. Marked decreases in κ_λ^* values from 1324 to 732 cm^2 g^{-1} and from 1098 to 858 cm^2 g^{-1} are observed in the wavelength range 300−440 nm for C-0.5 and C-1.0, respectively. C-3.5 showed the lowest absorption values of around 630 cm^2 g^{-1} with no large fluctuations in the entire range of λ.

The value of the specific scattering coefficient (σ_λ^*) was obtained by taking the difference of the specific absorption coefficient from the specific extinction coefficient ($\sigma_\lambda^* = \beta_\lambda^* - \kappa_\lambda^*$). As shown in Figure 5 (or Table S3 in the Supporting
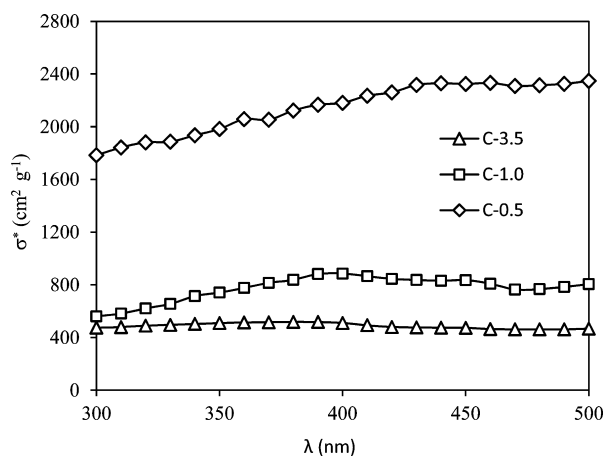
Figure 5. Specific scattering coefficient for the catalysts as a function of wavelength.

Information), differences between catalysts are also observed in the scattering contribution σ_λ^*, with the largest contribution corresponding to the C-0.5 catalyst (from 1780 to 3350 cm^2 g^{-1}) and the lowest one for the C-3.5 (from 450 to 500 cm^2 g^{-1}).

As it was already observed for the specific extinction coefficients, the values of κ_λ^* and σ_λ^* are intermediate between those of goethite (κ_λ^* from 93 to 115 cm^2 g^{-1} and σ_λ^* from 30 to 61 cm^2 g^{-1})[31] and ZVI (κ_λ^* from 15 474 to 21 568 cm^2 g^{-1} and σ_λ^* from 2528 to 7348 cm^2 g^{-1}).[17]

With regard to the asymmetry factor g_λ, Table S4 in the Supporting Information shows positive values over the whole range of wavelengths, which indicates a preferential forward direction of the scattered radiation. Small variations between the different values of g_λ were observed when comparing the three Fe-PILCs. Values are lower than those of goethite and ZVI.

In order to show the degree of accuracy attained by application of the DOM method and the nonlinear multi-parameter estimator, the experimental measurements of diffuse transmittance and diffuse reflectance as a function of wavelength can be compared with those predicted by the theoretical model of the RTE equation. As shown in Figure 6, the model reproduces with a high degree of accuracy the experimental values.

According to these results, optical properties of Fe-PILCs here studied are greatly dependent on their iron content. Light absorption is favored at low iron loadings and low wavelengths. This is a rather unexpected behavior since iron oxide is reported to undergo photoinduced electron transitions as in other semiconductor materials which are commonly used in photoassisted catalytic processes such as titanium dioxide, and
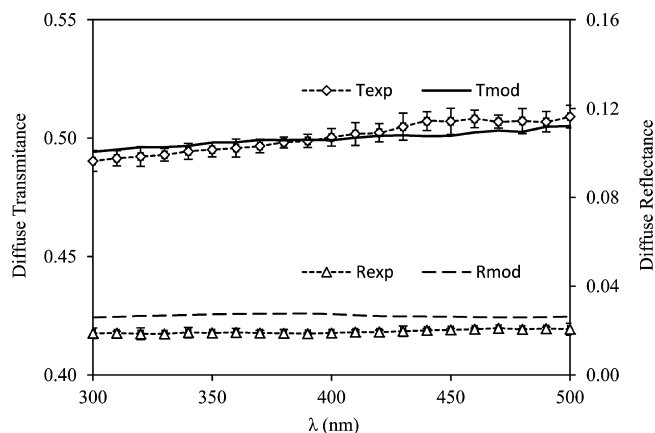
Figure 6. Comparison among predicted and measured values of diffuse transmittance and diffuse reflectance for a load of 1.0 g L^{-1} for C-3.5.

thereby photon absorption of Fe-PILCs should increase with their iron content.[41]

Optical properties of the Fe-PILCs are thus assumed to be affected to a higher extent by changes in textural properties when compared with those involving their iron oxide content, and the fact that values of κ_λ^* and σ_λ^* for a pure iron oxide under the form of goethite are even lower reinforces these assumptions. A more detailed study beyond the scope of this work should be performed to better understand the influence of textural properties of Fe-PILCs on their interactions with light.

Once the model has been optimized to estimate the values of κ_λ^*, σ_λ^*, and g_λ, the LVRPA can thus be calculated with eqs 4 and 5 for a given photoreactor on the basis of its configuration. Figure 7 shows LVRPA profiles in the cylindrical batch reactor
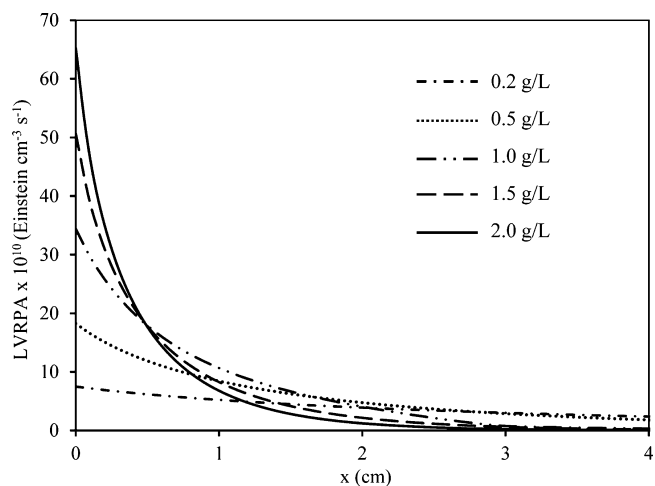
Figure 7. Spatial distribution of LVRPA in the photoreactor as a function of the characteristic spatial coordinate for different loads of C-3.5.

described in section 2. It can be observed how the LVRPA is affected by the characteristic spatial coordinate as well as the catalyst load. These results are of practical interest for reactor design because it allows determining the distance along the direction of radiation propagation where the photonic absorption rate becomes insignificant. As an example, the distance to attain 99% of total photonic absorption is approximately 2.5 cm for a catalyst load of 2.0 g L^{-1}.

In addition, the spatial average of the LVRPA in the reactor allows determination of the quantum efficiency (η) of the heterogeneous photo-Fenton process. The quantum efficiency can be defined as the ratio of the number of reactant molecules degraded or product molecules formed during a given time to the number of photons absorbed by the species to be activated, over the employed spectral range, during the same period of time.[42−44] As an example, the quantum efficiency for the degradation of 2-chlorophenol (2-CP) in photo-Fenton conditions with C-3.5 as catalyst was determined as follows:

$$\eta = \frac{C_{2\text{-CP},0} - C_{2\text{-CP},f}}{\langle e^a(x) \rangle_{V_R} (t_f - t_0)} \quad (12)$$

where $C_{2\text{-CP},0}$ is the initial molar concentration of 2-CP, $C_{2\text{-CP},f}$ is the final molar concentration of 2-CP, $(t_f - t_0)$ is the total time of the assay, and $\langle e^a(x) \rangle_{V_R}$ is the average value of LVRPA in the reactor calculated as

$$\langle e^a(x) \rangle_{V_R} = \frac{1}{V_R} \int_{V_R} e^a(x) \, dV \quad (13)$$

Table 4 shows the results obtained from assays performed in the reactor previously described for a period of 90 min. The

Table 4. Quantum Efficiency of the 2-CP Degradation for Different Loads of C-3.5

C_{cat} (g L^{-1})	$\langle e^a(x) \rangle_{V_R} \times 10^{10}$ (einstein cm^{-3} s^{-1})	$(C_{2\text{-CP},0} - C_{2\text{-CP},f})/(t_f - t_0) \times 10^{10}$ (mol cm^{-3} s^{-1})	η
0.2	2.76	0.118	0.043
1.0	3.34	0.556	0.167

initial concentration of 2-CP was 50 ppm, and the initial concentration of hydrogen peroxide was 265 ppm. The initial pH was adjusted to 3 with perchloric acid, and the temperature was maintained at 25 °C.

These results of quantum efficiency are useful for showing the possibility of using Fe-PILCs as catalysts to degrade the pollutant 2-CP by means of the heterogeneous photo-Fenton process.

4. CONCLUSIONS

Optical properties of Fe-PILCs containing different iron loadings were determined in the range of wavelength 300−500 nm by application of a method involving spectrophotometer measurements coupled with the solution of the radiative transfer equation (RTE). Significant differences in their optical properties are ascribed to differences in their textural properties. Fe-PILCs display photon absorption in all the range of wavelengths. The values obtained for κ_λ^* and σ_λ^* are intermediate between those of goethite and ZVI in the wavelength range studied. The positive values of g_λ indicate a preferential forward direction of the scattered radiation. Taking into account the different phenomena associated with light–catalyst interactions, mainly photon absorption and scattering, theoretical calculations can be made in order to determine the reactor design leading to the best results in terms of energy efficiency.

ASSOCIATED CONTENT

Ⓢ Supporting Information
Tables reporting the values of β_λ^*, κ_λ^*, σ_λ^*, and g_λ for the catalysts studied and values of β_λ^* and g_λ for goethite and ZVI.

This material is available free of charge via the Internet at http://pubs.acs.org.

AUTHOR INFORMATION

Corresponding Author
*E-mail: alfano@intec.unl.edu.ar.

Notes
The authors declare no competing financial interest.
§A.E.C.: Deceased July 12, 2014.

NOMENCLATURE

C = molar concentration (mol cm^{-3})
C_{cat} = catalyst load (g L^{-1})
DR = diffuse reflectance (dimensionless)
DT = diffuse transmittance (dimensionless)
e^a = local volumetric rate of photon absorption (einstein cm^{-3} s^{-1})
g = asymmetry factor (dimensionless)
G = incident radiation (einstein cm^{-2} s^{-1})
I = radiation intensity (einstein cm^{-2} s^{-1} sr^{-1})
L = spectrophotometric cell length
LVRPA = local volumetric rate of photon absorption
p = phase function (dimensionless)
s = linear coordinate along the direction $\underline{\Omega}$ (cm)
S_{BET} = specific surface area determined using the BET model (m^2 g^{-1})
t = time (s)
T = collimated transmittance (dimensionless)
$V_{\mu p}$ = specific micropore volume (cm^3 g^{-1})
V_R = reactor volume (cm^3)
V_T = specific total pore volume (cm^3 g^{-1})
x = axial coordinate (cm)
$\underline{x}$ = position vector (cm)

Greek Symbols
β = volumetric extinction coefficient (cm^{-1})
β_λ^* = specific extinction coefficient (cm^2 g^{-1})
δ = Dirac delta function
η = quantum efficiency (dimensionless)
θ = spherical coordinate (rad)
κ = volumetric absorption coefficient (cm^{-1})
κ_λ^* = specific absorption coefficient (cm^2 g^{-1})
λ = wavelength (nm)
μ = direction cosine of the ray for which the RTE is written
μ' = direction cosine of an arbitrary ray before scattering
μ_0 = cosine of the angle between the direction of the incident and the scattered rays
σ = volumetric scattering coefficient (cm^{-1})
σ_λ^* = specific scattering coefficient (cm^2 g^{-1})
Ω = solid angle (sr)
$\underline{\Omega}$ = unit vector in the direction of radiation propagation

Γ = global wall reflection coefficient (dimensionless)

Subscripts

0 = inlet condition
f = final condition
λ = dependence on wavelength

■ REFERENCES

(1) Ameta, R.; Kumar, A.; Punjabi, P. B.; Ameta, S. C. Advanced oxidation processes. In *Wastewater Treatment Advanced Processes and Technologies*; Rao, D. G., Senthikumar, R., Byrne, J. A., Feroz, S., Eds.; CRC Press: Boca Raton, FL, 2012.

(2) Comninellis, C.; Kapalka, A.; Malato, S.; Parson, S. A.; Poulios, I.; Mantzavinos, D. Perspective Advanced oxidation processes for water treatment: advances and trends for R&D. *J. Chem. Technol. Biotechnol.* **2008**, *83*, 769.

(3) Litter, M. I. Introduction to Photochemical Advanced Oxidation Processes for Water Treatment. In *Environmental Photochemistry Part II*; Boule, P., Bahnemann, D. W., Robertson, P. K. J., Eds.; Springer: Berlin, 2005.

(4) Legrini, O.; Oliveros, E.; Braun, A. M. Photochemical process for water treatment. *Chem. Rev.* **1993**, *93*, 671.

(5) Bautista, P.; Mohedano, A. F.; Casas, J. A.; Zazo, J. A.; Rodriguez, J. J. An overview of the application of Fenton oxidation to industrial wastewaters treatment. *J. Chem. Technol. Biotechnol.* **2008**, *83*, 1323.

(6) Fenton, H. J. H. Oxidation of tartaric acid in presence of iron. *J. Chem. Soc., Trans.* **1894**, *65*, 899.

(7) Safarzadeh-Amiri, A.; Bolton, J. R.; Cater, S. R. The use of iron in advanced oxidation processes. *J. Adv. Oxid. Technol.* **1996**, *1*, 18.

(8) Malato, S.; Blanco, J.; Vidal, A.; Richter, C. Photocatalysis with solar energy at a pilot-plant scale: an overview. *Appl. Catal., B* **2002**, *37*, 1.

(9) Ayodele, O. B.; Lim, J. K.; Hameed, B. H. Pillared montmorillonite supported ferric oxalate as heterogeneous photo-Fenton catalyst for degradation of amoxicillin. *Appl. Catal., A* **2012**, *413−414*, 301.

(10) Catrinescu, C.; Arsene, D.; Apopei, P.; Teodosiu, C. Degradation of 4-chlorophenol from wastewater through heteroneous Fenton and photo-Fenton process, catalyzed by Al-Fe PILC. *Appl. Clay Sci.* **2012**, *58*, 96.

(11) Deng, C.; Ren, C.; Wu, F.; Deng, N.; Glebov, E.; Pozdnyakov, I.; Plyusnin, V. Montmorillonite KSF as catalyst for degradation of acetaminophen with heterogeneous Fenton reactions. *React. Kinet., Mech. Catal.* **2010**, *100*, 277.

(12) Gonzalez-Olmos, R.; Martin, M.; Georgi, A.; Kopinke, F.; Oller, I.; Malato, S. Fe-zeolites as heterogeneous catalysts in solar Fenton-like reactions at neutral pH. *Appl. Catal., B* **2012**, *125*, 51.

(13) Herney-Ramirez, J.; Vicente, M. A.; Madeira, L. M. Heterogeneous photo-Fenton oxidation with pillared clay-based catalysts for wastewater treatment: A review. *Appl. Catal., B* **2010**, *98*, 10.

(14) Huang, Ch.-P.; Huang, Y.-H. Application of an active immobilized iron oxide with catalytic H_2O_2 for the mineralization of phenol in a batch photo-fluidized bed reactor. *Appl. Catal., A* **2009**, *357*, 135.

(15) Liu, T.; You, H. Photoassisted Fenton-like degradation of polyacrylamide aqueous solutions using iron oxide/TiO_2/Al_2O_3 heterogeneous catalysts. *React. Kinet., Mech. Catal.* **2013**, *109*, 233.

(16) Ortiz de la Plata, G. B.; Alfano, O. M.; Cassano, A. E. Decomposition of 2-CP employing goethite as Fenton catalyst. I. Proposal of a feasible combined reaction scheme of heterogeneous and homogeneous reaction. *Appl. Catal., B* **2010**, *95*, 1.

(17) Ortiz de la Plata, G. B.; Alfano, O. M.; Cassano, A. E. 2-Chlorophenol degradation via photo Fenton reaction employing zero valent iron nanoparticles. *J. Photochem. Photobiol., A* **2012**, *233*, 53.

(18) Son, V.; Im, J. K.; Zoh, K. D. A Fenton-like degradation mechanism for 1,4-dioxane using zero-valent iron (Fe0) and UV light. *Water Res.* **2009**, *43*, 1457.

(19) Soon, A. N.; Hameed, B. H. Degradation of Acid Blue 29 in visible light radiation using iron modified mesoporous silica as heterogeneous Photo-Fenton catalyst. *Appl. Catal., A* **2013**, *450*, 96.

(20) Zhong, X.; Royer, S.; Zhang, H.; Huang, Q.; Xiang, L.; Valange, S.; Barrault, J. Mesoporous silica iron-doped as stable and efficient heterogeneous catalyst for the degradation of C.I. Acid Orange 7 using sono-photo-Fenton process. *Sep. Purif. Technol.* **2011**, *80*, 163.

(21) Hou, M.; Ma, C.; Zhang, W.; Tang, X.; Fan, Y.; Wan, H. Removal of rhodamine B using iron-pillared bentonite. *J. Hazard. Mater.* **2011**, *186*, 1118.

(22) Zhang, S.; Liang, S.; Wang, X.; Long, J.; Li, Z.; Wu, L. Trinuclear iron cluster intercalated montmorillonite catalyst: Microstructure and photo-Fenton performance. *Catal. Today* **2011**, *175*, 362.

(23) Bouras, O.; Bollinger, J.; Baudu, M.; Khalaf, H. Adsorption of diuron and its degradation products from aqueous solution by surfactant-modified pillared clays. *Appl. Clay Sci.* **2007**, *37*, 240.

(24) Galeano, L. A.; Vicente, M. A.; Gil, A. Treatment of municipal leachate of landfill by Fenton-like heterogeneous catalytic wet peroxide oxidation using an Al/Fe-pillared montmorillonite as active catalyst. *Chem. Eng. J.* **2011**, *178*, 146.

(25) Chen, Z.; Jiao, Z.; Pan, D.; Li, Z.; Wu, M.; Shek, C.-H.; Wu, C. M. L.; Lai, J. K. L. Recent Advances in Manganese Oxide Nanocrystals: Fabrication, Characterization, and Microstructure. *Chem. Rev.* **2012**, *112*, 3833.

(26) Liu, Y.; Chen, Z.; Shek, C.-H.; Wu, C. M. L.; Lai, J. K. L. Hierarchical Mesoporous MnO_2 Superstructures Synthesized by Soft-Interface Method and Their Catalytic Performances. *ACS Appl. Mater. Interfaces* **2014**, *6*, 9776.

(27) Ozisik, M. N. *Radiative Transfer and Interactions with Conduction and Convection*; Wiley: New York, 1973.

(28) Cassano, A. E.; Martín, C. A.; Brandi, R. J.; Alfano, O. M. Photoreactor analysis and design: fundamentals and applications. *Ind. Eng. Chem. Res.* **1995**, *34*, 2155.

(29) Cabrera, M. I.; Alfano, O. M.; Cassano, A. E. Absorption and scattering coefficients of titanium dioxide particulate suspensions in water. *J. Phys. Chem.* **1996**, *100*, 20043.

(30) Marugan, J.; Van Grieken, R.; Alfano, O. M.; Cassano, A. E. Optical and Physicochemical Properties of Silica-Supported TiO_2 Photocatalysts. *AIChE J.* **2006**, *52*, 2832.

(31) Ortiz de la Plata, G. B.; Alfano, O. M.; Cassano, A. E. Optical properties of goethite catalyst for heterogeneous photo-Fenton reactions. Comparision with a titanium dioxide catalyst. *Chem. Eng. J.* **2008**, *137*, 396.

(32) Satuf, M. L.; Brandi, R. L.; Cassano, A. E.; Alfano, O. M. Experimental method to evaluate the optical properties of aqueous titanium dioxide suspensions. *Ind. Eng. Chem. Res.* **2005**, *44*, 6643.

(33) De León, A.; Castiglioni, J.; Bussi, J.; Sergio, M. Catalytic activity of an iron pillared montmorillonite clay mineral in a heterogeneous photo-Fenton process. *Catal. Today* **2008**, *133−135*, 600.

(34) De León, A.; Sergio, M.; Bussi, J. Iron-pillared clays as catalysts for dye removal by the heterogeneous photo-Fenton technique. *React. Kinet., Mech. Catal.* **2013**, *110*, 101.

(35) De León, A.; Sergio, M.; Bussi, J.; Ortiz de la Plata, G.; Cassano, A.; Alfano, O. Application of a montmorillonite clay modified with iron in photo-Fenton process. Comparison with goethite and nZVI. *Environ. Sci. Pollut. Res.* **2014**, DOI: 10.1007/s11356-014-2681-6.

(36) Diano, W.; Rubino, R.; Sergio, M. Al-pillared montmorillonite: Preparation from concentrated slurries of homoionic Ca clay, characterization and thermal stability. *Microporous Mesoporous Mater.* **1994**, *2*, 179.

(37) Yamanaka, S.; Doi, T.; Sako, S.; Hattori, M. High surface area solids obtained by intercalation of iron oxide pillars in montmorillonite. *Mater. Res. Bull.* **1984**, *19*, 161.

(38) Duderstadt, J. J.; Martin, R. *Transport Theory*; Wiley: New York, 1979.

(39) Ortiz de la Plata, G. B.; Alfano, O. M.; Cassano, A. E. Decomposition of 2-CP employing goethite as Fenton catalyst. I. Reaction kinetics of the heterogeneous Fenton and photo-Fenton mechanisms. *Appl. Catal., B* **2010**, *95*, 14.

(40) Pouet, M.-F.; Azema, N.; Touraud, E.; Thomas, O. Physical and Aggregate Properties. In *UV-Visible Spectrophotometry of Water and Wastewater*; Thomas, O., Burgess, C., Eds.; Elsevier: Amsterdam, The Netherlands, 2007.

(41) Bakardjieva, S.; Stengl, V.; Subrt, J.; Houskova, V.; Kalenda, P. Photocatalytic efficiency of iron oxides: Degradation of 4-chlorophenol. *J. Phys. Chem. Solids* **2007**, *68*, 721.

(42) Braslavsky, S. E.; Braun, A. M.; Cassano, A. E.; Emeline, A. V.; Litter, M. I.; Palmisano, L.; Parmon, V. N.; Serpone, N. Glossary of terms used in photocatalysis and radiation catalysis (IUPAC Recommendations 2011). *Pure Appl. Chem.* **2011**, *83*, 931.

(43) Benzaquén, T. B.; Isla, M. A.; Alfano, O. M. Quantum Efficiencies of the Photo-Fenton Degradation of Atrazine in Water. *Water Sci. Technol.* **2012**, *66*, 2209.

(44) Conte, L. O.; Querini, P.; Albizzati, E. D.; Alfano, O. M. Photonic and Quantum Efficiencies for the Homogeneous Photo-Fenton Degradation of Herbicide 2,4-D using Different Iron Complexes. *J. Chem. Technol. Biotechnol.* **2014**, *89*, 1967.